XV International Conference on Computational Plasticity. Fundamentals and Applications
COMPLAS 2019
E. Oñate, D.R.J. Owen, D. Peric, M. Chiumenti & Eduardo de Souza Neto (Eds)

MODELLING ACID ATTACK OF OIL-WELL CEMENT EXPOSED TO CARBONATED BRINE: EFFECT OF SPECIMEN GEOMETRY ON EXPERIMENTAL RESULTS

L. BARANDIARÁN, J. LIAUDAT, C. M. LÓPEZ AND I. CAROL

School of Civil Engineering of Barcelona (ETSECCPB)
Universitat Politècnica de Catalunya
Campus Nord UPC, 08034 Barcelona, Spain
e-mail: lucia.barandiaran@upc.edu, joaquin.liaudat@upc.edu, carlos.maria.lopez@upc.edu, ignacio.carol@upc.edu

Key words: Carbon sequestration, Oil-well cement, CO_2, Carbon dioxide, Acid attack, Chemical model, Finite Element Method

Abstract. In recent years, the authors and co-workers have developed a diffusion-reaction model for the degradation process of oil-well cements exposed to carbonated brines in the context of CO_2 capture and storage in abandoned oil reservoirs. The model considers two main diffusion-reaction field variables for the concentrations of aqueous calcium and carbon species in the pore solution of the hardened cement paste, complemented by two diffusion-only field variables for chloride and alkalis concentrations. The volume fractions of solid constituents evolve according to the chemical kinetics and chemical equilibrium equations of the reactions involved, determining the diffusivity properties of the material. In this paper, in the framework of an experimental campaign in preparation, this model is used for assessing the effect of different specimen geometries on the kinetics and extent of the acid attack. The results obtained will help to optimize the experimental setup and to the interpretation of the results obtained.

1 INTRODUCTION

Geologic carbon dioxide (CO_2) sequestration represents an effective mitigation action for the stabilization of greenhouse gas concentrations in the atmosphere. The solution consists of the capture and storage of CO_2 generated by industrial processes in geological formations [1]. Among other possibilities, depleted oil and gas fields emerge as the most promising options, mainly because the oil and gas that originally accumulated in the fields traps did not escape for millions of years demonstrating their integrity and safety. However, the presence of abandoned wells that perforate the cap rock may jeopardize the integrity of many mature reservoirs by constituting potential CO_2 leakage pathways [2]. In particular, the long-term chemical stability of the oil-well cements may be affected by the changes in the exposure conditions induced by the CO_2 injections. When ordinary

portland cements, which are alkaline in nature, are exposed to the carbonic acid resulting from the CO_2 dissolution in the water filling the depleted reservoir, a dissolution reaction occurs leading to the decalcification of the cement, with consequent increase of porosity and lost of mechanical strength [3, 4].

In this context, the necessity arises of experimental studies and numerical models for an accurate assessment of the long-term sealing capacity of oil-well cements in the context of carbon sequestration projects. In a previous paper, Liaudat et al. [5] presented a diffusion-reaction model capable of successfully simulating experimental results of Hardened Cement Paste (HCP) degradation of cylindrical samples, carried out by Duguid and Scherer [6]. In a subsequent stage, this diffusion-reaction model is being coupled with a geomechanical model, in order to study possible chemo-mechanical degradation mechanisms of the oil-well cements. For this purpose and as part of the same research project, the fracture mechanical parameters of the degraded HCP will be characterized by means of laboratory experimental tests. In these experiments, prismatic HCP specimens with a central notch will be exposed to a carbonated brine for different time lapses, after which they will be mechanically tested in a three-point bending scheme. With the aim of determining the best notch geometry in order to optimize the time required to produce significant degradation of the HCP around the notch tip, a number of simulations are performed using the model by Liaudat et al. [5]. Additionally, the simulations make it possible to have an estimate of the rate at which calcium is released from the HCP specimens to the chemical reactor, a result which will help to dimension the equipment to be used in the experimental campaign. This paper presents the results obtained in this study.

2 THE MODEL

In the following paragraphs, the diffusion-reaction model proposed by Liaudat et al. [5] is briefly summarized.

2.1 Diffusion-reaction mechanism

As CO_2 dissolves in the brine within the reservoir, carbonic acid (H_2CO_3) is formed and subsequently dissociated mainly into HCO_3^- and CO_3^{2-} (Reactions (1) and (2)). As carbon concentration rises, a diffusion process is generated from the brine into the HCP, increasing the acidity of pore solution in the HCP. In this condition, the portlandite ($Ca(OH)_2$) in contact with the pore solution becomes unstable, dissolving into Ca^{2+} (Reaction (3) towards right). As long as some portlandite remains in contact with the pore solution, the pH will remain high and, consequently, the predominant carbon species will be CO_3^{2-}. Then, the Ca^{2+} ions will react with the CO_3^{2-} ions to form solid calcite (Eq. (4) towards left) within the pore space, locally reducing the porosity of the material. If the carbon concentration in pore solution continues rising, portlandite will be completely depleted and the pH of the pore solution will significantly decline. In consequence, the calcite production will be slowed down and the $CSH_{2.5}$ (cement chemistry notation) will also become unstable, releasing Ca^{2+} to the pore solution (Reaction (5) towards left). For

an additional increment of carbon concentration, further decline of pH will be induced, triggering calcite dissolution (Reaction (4) towards right) and complete decalcification of the $CSH_{2.5}$ (Reaction (5) towards left). The remaining amorphous silicate hydrates $SH_{1.5}$ is considered to be stable in the acidic carbonated brine. In this condition, HCP is totally degraded exhibiting complete mechanical strength loss and high permeability.

$$CO_{2(aq)} + H_2O \leftrightharpoons HCO_3^- + H^+ \tag{1}$$
$$HCO_3^- \leftrightharpoons CO_3^{2-} + H^+ \tag{2}$$
$$Ca(OH)_{2(s)} \leftrightharpoons Ca^{2+} + 2OH^- \tag{3}$$
$$CaCO_{3(s)} \leftrightharpoons Ca^{2+} + CO_3^{2-} \tag{4}$$
$$[Ca(OH)_2][(SiO_2)(H_2O)_{1.5}]_{(s)} \leftrightharpoons Ca^{2+} + 2OH^- + (SiO_2)(H_2O)_{1.5(s)} \tag{5}$$
$$H_2O \leftrightharpoons OH^- + H^+ \tag{6}$$

2.2 Formulation and numerical implementation

The model considers two main diffusion-reaction field equations for the concentrations of aqueous calcium and carbon species in the pore solution of the HCP, complemented by two diffusion-only field variables for chloride and alkalis concentrations, namely:

$$\frac{\partial(\phi c^{ca})}{\partial t} = \nabla(D^{ca}\nabla c^{ca}) + q^{ca} \tag{7}$$
$$\frac{\partial(\phi c^{tc})}{\partial t} = \nabla\left(D^{tc}\nabla c^{tc}\right) + q^{tc} \tag{8}$$
$$\frac{\partial\left(\phi c^{cl}\right)}{\partial t} = \nabla\left(D^{cl}\nabla c^{cl}\right) \tag{9}$$
$$\frac{\partial(\phi c^{r})}{\partial t} = \nabla(D^{r}\nabla c^{r}) \tag{10}$$

where superscripts ca, tc, cl, and r specify calcium, total carbon, chloride, and alkali species, respectively, ϕ is the total porosity, c^β [mol/m^3] is the concentration of aqueous β-species in the pore solution, D^β [m^2/s] is the effective diffusivity of aqueous β-species in the porous medium, and q^β [mol/(m$^3 \cdot$ s)] is the rate of production/consumption of β-species per unit volume of porous medium, which also is a function of the concentration of aqueous species, i.e. $q^\beta = q^\beta(c^{ca}, c^{tc}, c^{cl}, c^r)$, and $\nabla = [\partial/\partial x \ \ \partial/\partial y]^{\mathrm{T}}$. The variable c^{tc} stands for the sum of molar concentrations of each carbonic species present in pore solution, i.e. $c^{tc} = c^{c0} + c^{c1} + c^{c2}$, where $c0$, $c1$ and $c2$ stand for $CO_{2(aq)}$, HCO_3^- and CO_3^{2-}, respectively. Note that the only transport mechanism considered is the Fickian diffusion of the aqueous species. The sink/source terms q^β in Eqs. (7) and (8) are determined by net rates of production/dissolution of the reactive solid species, namely portlandite, calcite, $CSH_{2.5}$ and SH, according to Reactions (3), (4) and (5). In turn, the volume balance of the solid species determine the evolution of the porosity and of the effective diffusivities D^β of the material. The total volume of pore space filled with pore solution includes both the volume of capillary pores and the volume of gel pores within the $CSH_{2.5}$ and SH volume fractions.

It is assumed that the driving force of the dissolution/precipitation reaction of reactive solid α-species is $(1 - \psi^{\alpha})$, where ψ^{α} is the dimensionless saturation index of the pore solution with respect to the solid α-species. Depending on whether $\psi^{\alpha} > 1$, $\psi^{\alpha} = 1$, or $\psi^{\alpha} < 1$, the pore solution is over-saturated, in equilibrium, or under-saturated, respectively, with respect to α-species. The saturation indices are functions of the activities of the primary and secondary aqueous species involved in the corresponding chemical reaction, which are estimated with the well-known Davies equation using the modification on the second term as proposed by Samson and Lemaire [7]. In order to determine the concentration of secondary species, additional calculations need to be performed considering the equilibrium equations of the dissociation Reactions (1), (2) and (6), as well as the electric charge neutrality of the pore solution.

A modified version of the analytical formula proposed by Oh and Jang [8] is used to compute the effective diffusivity of the primary aqueous β-species in the water-saturated HCP (D^{β}). The equation involves four parameters which describe the microstructure of HCP: capillary porosity, percolation threshold, the normalized diffusivity of solid phase, and the percolation exponent. Reduction of tortuosity in pore structure due to $CSH_{2.5}$ dissolution is considered by assuming that the percolation exponent evolves with the decalcification of the $CSH_{2.5}$.

Isothermal and isobaric conditions are assumed at all times, as well as water saturation of the material pores.

The model has been implemented in the Finite Element code DRACFLOW, in-house developed by the group of Mechanics of Materials at UPC (MECMAT/UPC). Formerly, the code has been used to model durability problems in concrete such as drying shrinkage [9], external sulfate attack [10], Alkali-Silica Reaction [11], and high temperatures [12].

3 MODELLING RESULTS

3.1 Model geometry and parameters

For the experimental campaign described in the introduction, prismatic 40 × 40 × 160 mm HCP specimens will be used (Fig. 1a). The specimens will have a central notch to localize fracture in a three-point bending test. In order to optimize the experimental setup, three different possible notch geometries are studied in this paper: 2 × 20 mm rectangular notch, 2 × 10 mm rectangular notch, and a Chevron type notch with the dimensions indicated in Fig. 1b. After curing, the external surfaces of the specimens will be covered with a layer of epoxy resin in order to prevent the acid attack of these zones. In the case of the rectangular notches, all the internal surfaces will remain uncovered, while in the case of the Chevron notch only the 'tip' of the notch will remain uncovered. Under these conditions, the acid attack process may be simulated with two-dimensional geometries as the one schematically represented for the Chevron notch specimen in Fig. 1b, taking advantage of the symmetry plane indicated in Fig. 1a. The models have been spatially discretized with quadrangular linear elements representing the brine and HCP domains, and zero-thickness interface elements representing the brine-HCP interfaces and the internal layer of epoxy in the Chevron notch specimen (Fig. 1b). Simulations have

been performed for a total time of 600 hours (25 days), discretized in increments of 0.2 hours.

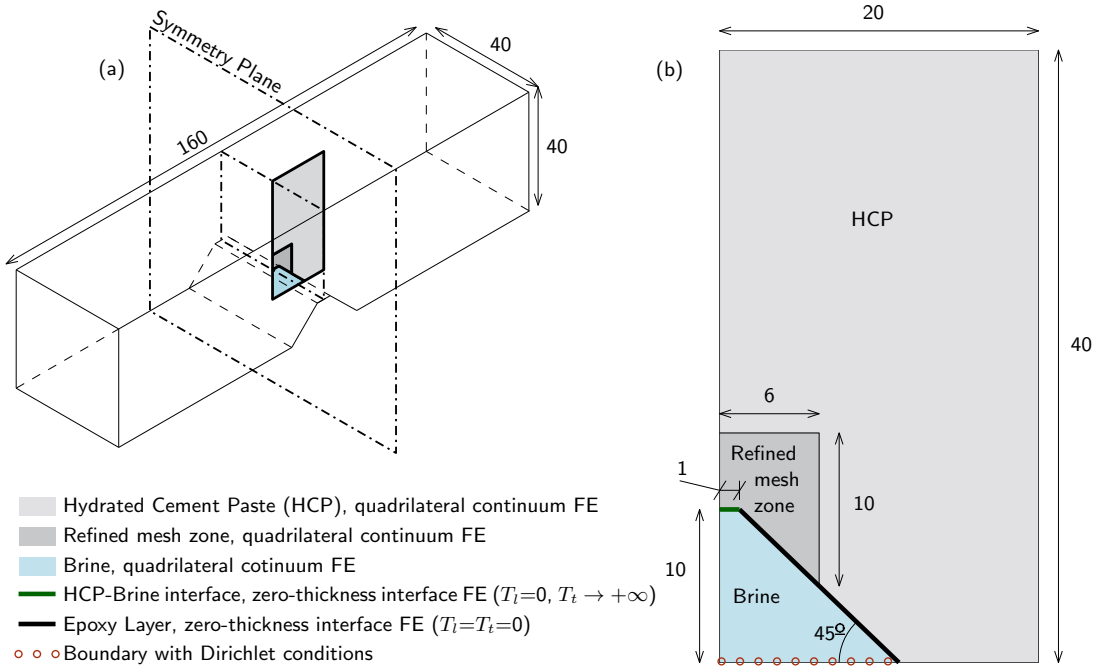

Figure 1: (a) Prismatic specimen geometry. (b) Model geometry and diffusion boundary conditions. Dimensions given in mm.

The specimens will be prepared with cement CEM I 42,5 N-SR 5 [16] and with a water to cement ratio of 0.45. After casting, the specimens will be cured in 0.5 M NaCl brine at 50 °C for 28 days. The initial volume fractions in the HCP are estimated using the expressions given by Brouwers [14, 15], and taking into account the effects of the curing temperature on the gel porosity of the C–S–H reported by Gallucci et al. [17], obtaining the following volume fractions: $CSH_{2.5}$ = 0.206, portlandite = 0.243, Inert Cement Paste = 0.235, Capillary Pores = 0.315, and total (gel + capillary) pores = 0.428.

It is assumed that at the beginning of the exposure to the carbonated brine, the concentrations of alkali and chlorides are homogeneous in the specimens and equal to that of the curing brine, i.e. $c_o^{cl} = c_o^r = 500$ mmol/L. The initial concentration of calcium in pore solution is determined as the saturation concentration of portlandite in 0.5 M NaCl solution at 20 °C, resulting in $c_o^{ca} = 20.95$ mmol/L.

In the reactors, the specimens will be exposed to 0.5 M NaCl solution at 20 °C, saturated with CO_2 at a constant pressure of 1.5 MPa. The total carbon concentration in the brine under these conditions is estimated using the semi-empirical thermodynamic model proposed by Dubacq et al. [13], resulting in 493 mmol/L. Since the brine in the reactor will be continuously renovated, Dirichlet boundary conditions are imposed at the 'mouth' of the notches with $\hat{c}^{ca} = 0$ mmol/L, $\hat{c}^{tc} = 493$ mmol/L, $\hat{c}^{cl} = 500$ mmol/L, and $\hat{c}^r = 500$ mmol/L.

The saturation product constants considered for Reactions (3), (4), and (5) are K_{sp}^{CH} = 7.515E−09, $K_{sp}^{C\bar{C}}$ = 3.554E−09 and K_{sp}^{CSH} = 7.515E−09, for activities in mol/L. The equilibrium constants considered for Reactions (1), (2), and (6) are K_{eq}^{c0}= 4.136E−07, K_{eq}^{c1}= 4.246E−11 and K_{eq}^{w} = 6.893E−15, also for activities in mol/L.

3.2 Results

Figures 2 and 3 show the concentrations of carbon species and calcium in pore solution, respectively, for three different exposure times and for each of the notch geometries considered. Similarly, Figs. 4 and 5 show the volume fractions of portlandite and calcite, respectively, for the same exposure times and notch geometries. The molar rate of calcium leaving the specimen through the notch 'mouth', i.e. the sum of the reactions to the Dirichlet boundary conditions imposed to the nodes at the notch mouth, is plotted as a function of time for each notch geometry in Fig. 6.

In the specimens with rectangular notch, the degradation process progresses mainly in the area close to the notch mouth (where the Dirichlet boundary conditions are applied) and in the horizontal direction. The degradation of the notch tip is slowed down mainly because of two reasons: (i) most of the carbon species flowing into the notch are captured in the formation of calcite in the notch mouth zone, leaving only a small remnant to attack the notch tip zone (Fig. 2); (ii) as calcium ions are released into the notch from the lateral surfaces, the calcium concentration is locally risen reducing or even inverting the calcium concentration gradient from the tip to the mouth of the notch (Fig. 3). These effects are more clearly observed for the 20-mm notch, but can be also be appreciated for the 10-mm notch. In contrast, in the specimen with the Chevron notch and the internal lateral surfaces covered with epoxy resin, none of these mechanisms are developed and, consequently, the degradation front at the notch tip zone progresses at a significantly higher velocity. It must be noted that the better performance of the Chevron notch specimen is mainly because of the layer of epoxy resin covering the internal lateral surface rather than because of the Chevron geometry itself.

Since, from the point of view of the experimental tests that motivated this numerical study (see Sec. 1), the main interest is maximizing the velocity of advancement of the degradation front at the notch tip zone of the specimens, the Chevron notch emerges as the best option. Furthermore, the rate at which calcium is released from the Chevron notch specimen is less than a half of that of the specimens with rectangular notch (Fig. 6). This implies that specimens with Chevron notch will require a much lower flow of fresh carbonated brine in order to keep the calcium concentration in the reactor under a certain maximum value.

4 CONCLUDING REMARKS

- In the context of an experimental campaign in preparation, the diffusion-reaction model developed by Liaudat et al. [5] has been used for preliminary assessing different possible notch geometries for $40 \times 40 \times 160$ mm prismatic specimens to be used in three-point bending tests after being exposed to carbonated brine.

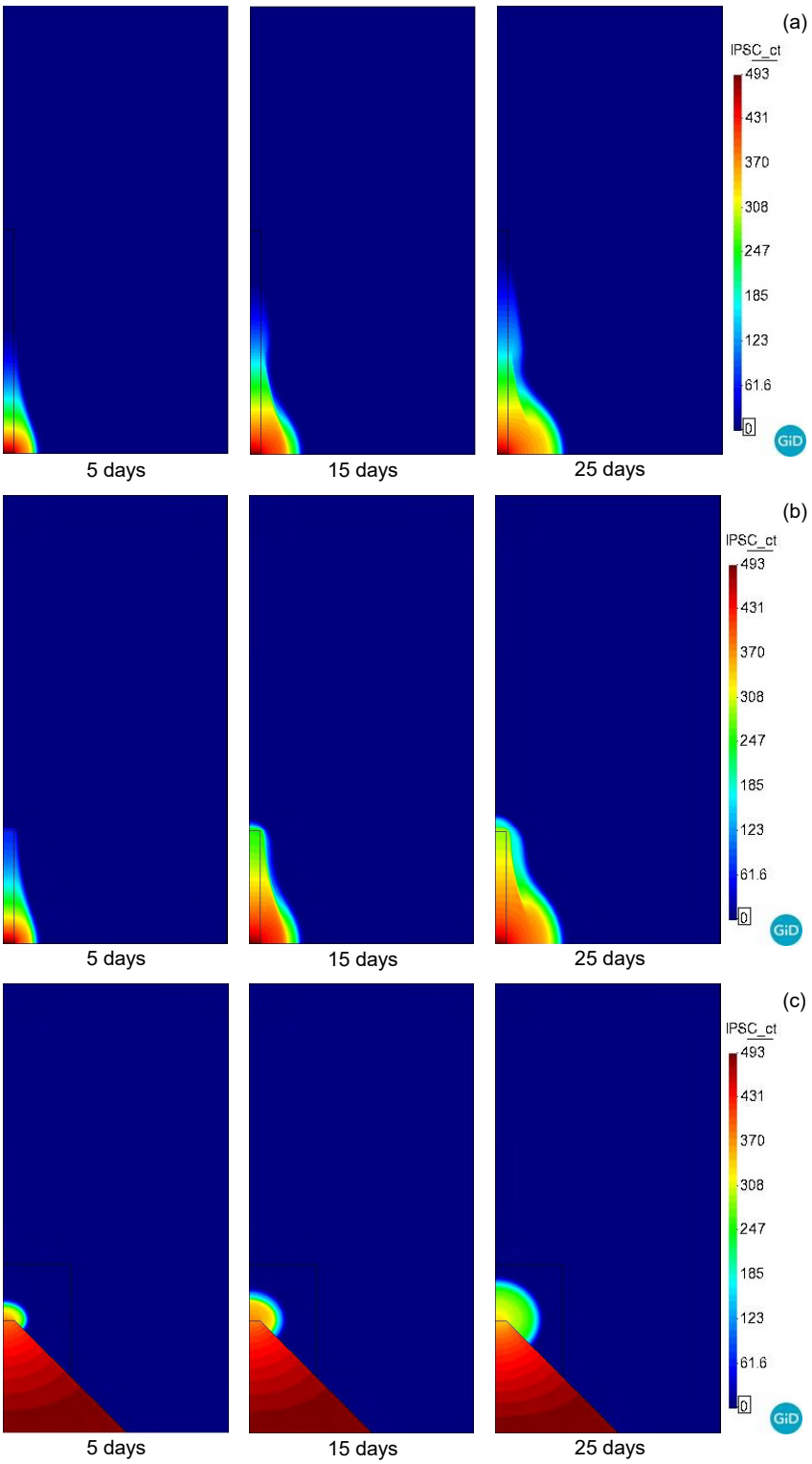

Figure 2: Concentration of carbon species in pore solution [mmol/L]. (a) 2 × 20 mm rectangular notch. (b) 2 × 10 mm rectangular notch. (c) Chevron type notch.

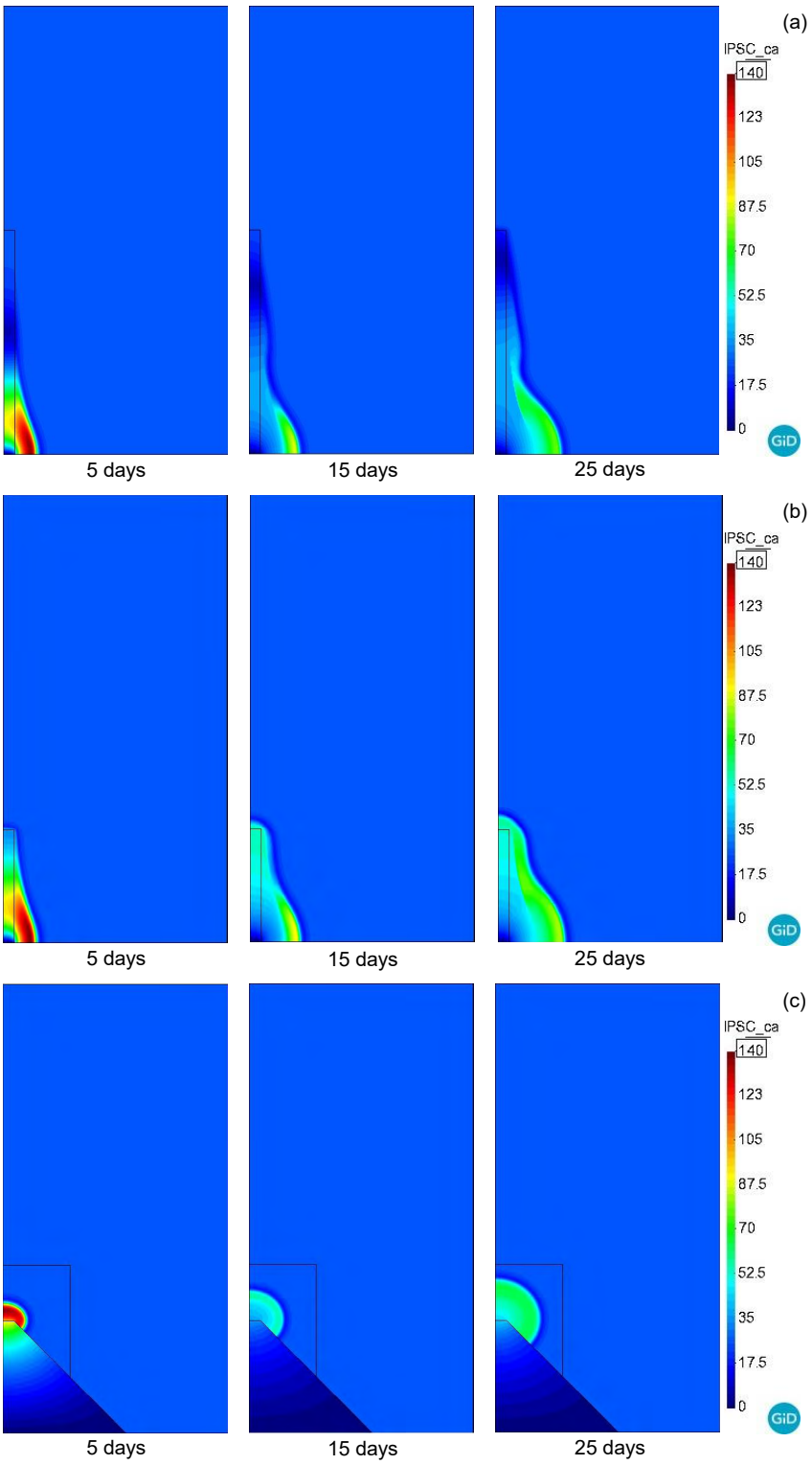

Figure 3: Calcium concentration in pore solution [mmol/L]. (a) 2×20 mm rectangular notch. (b) 2×10 mm rectangular notch. (c) Chevron type notch.

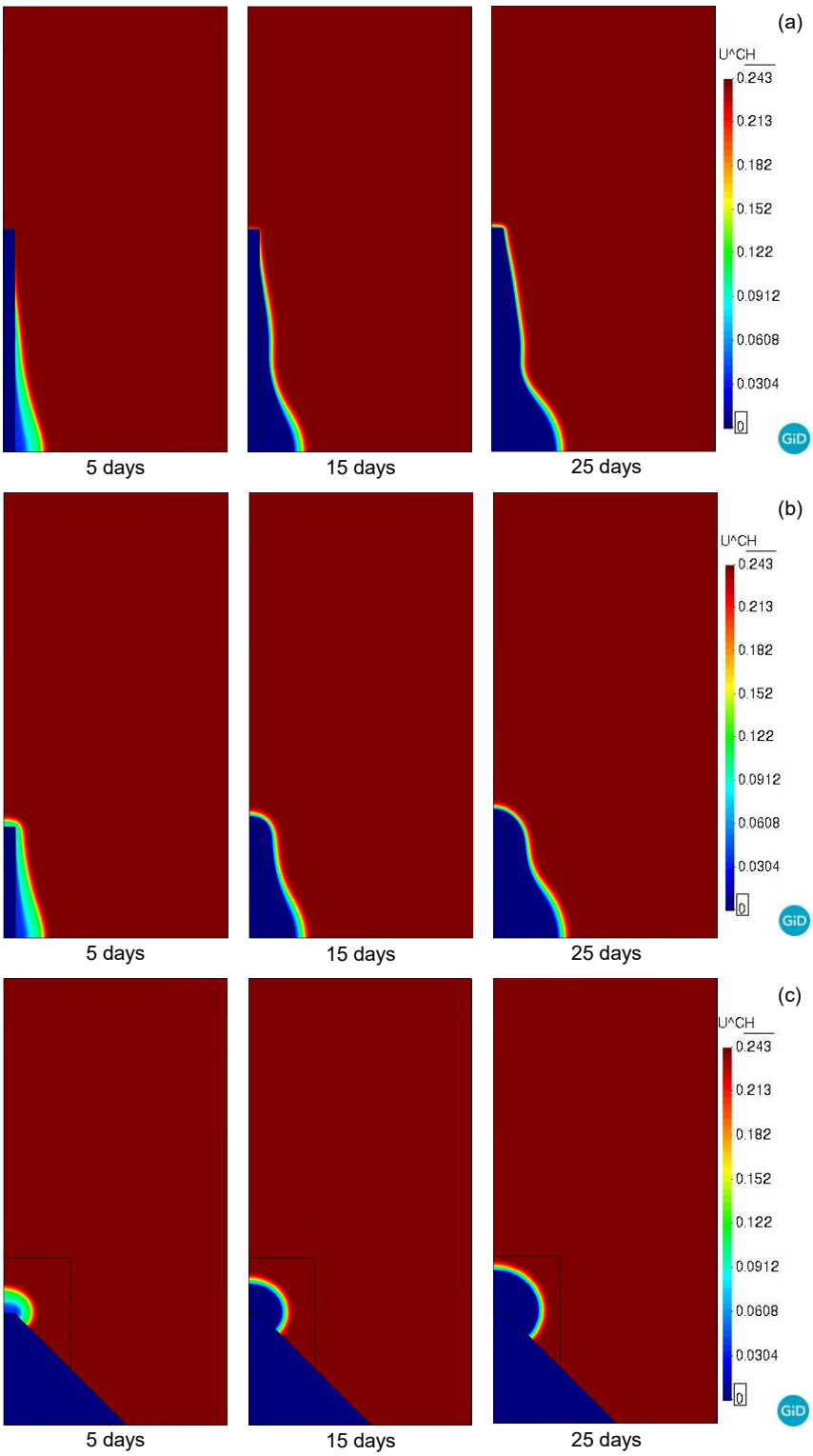

Figure 4: Portlandite volume fraction [m^3/m^3]. (a) 2×20 mm rectangular notch. (b) 2×10 mm rectangular notch. (c) Chevron type notch.

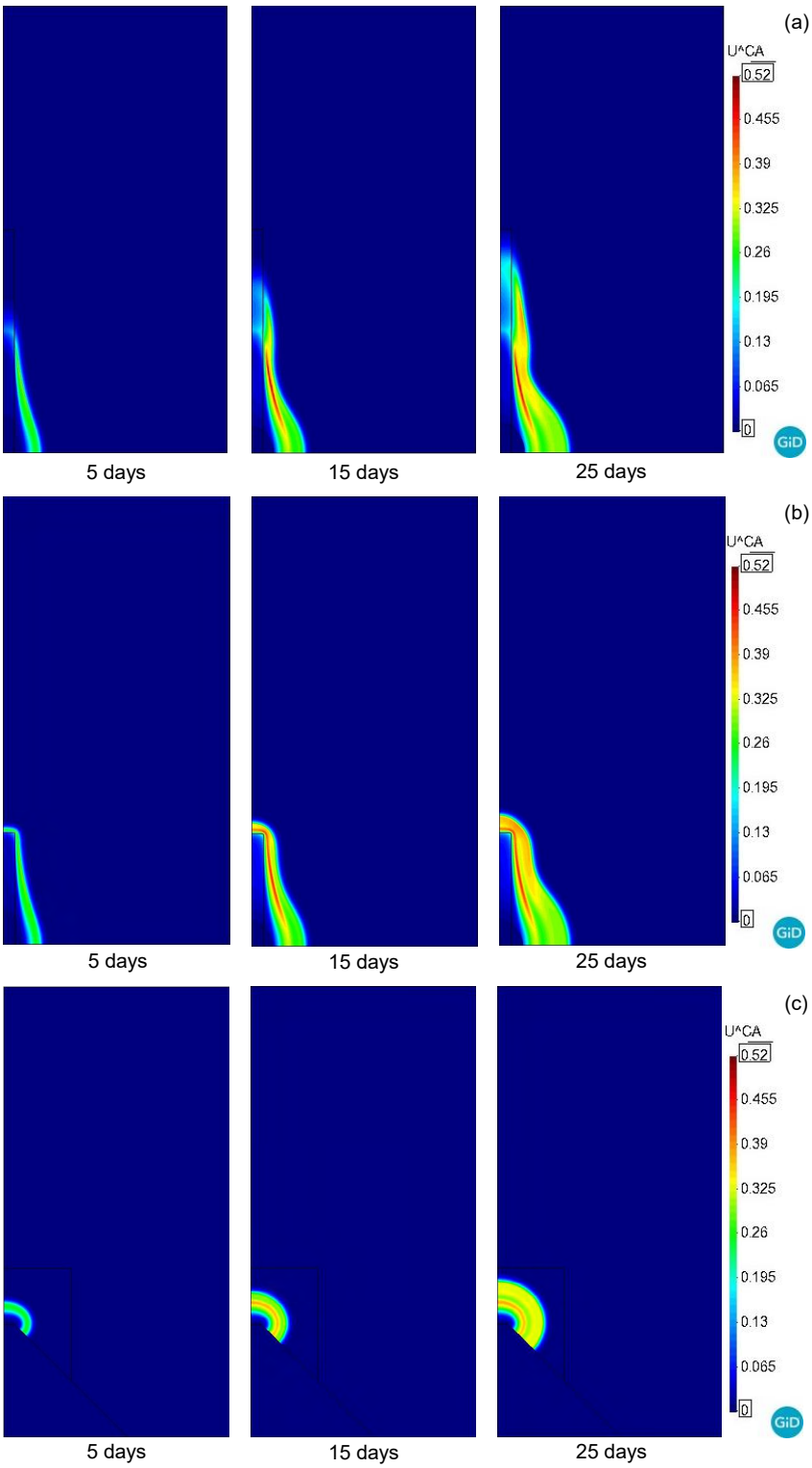

Figure 5: Calcite volume fraction [m^3/m^3]. (a) 2×20 mm rectangular notch. (b) 2×10 mm rectangular notch. (c) Chevron type notch.

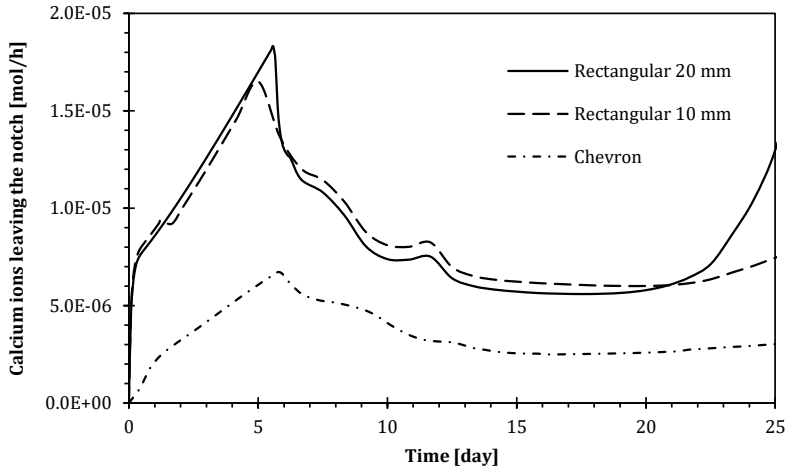

Figure 6: Molar rate of calcium ions leaving the notch at nodes with Dirichlet boundary conditions. Results have been multiplied by 2 and by 0.40 in order to represent the calcium released by a full-size prismatic specimen.

- The simulations have helped to identify the mechanisms determining the advancement velocity of the degradation front at the zone of interest (notch tip zone) in specimens with rectangular notches, leading to the adoption of a more convenient Chevron type notch geometry.

- The simulations have provided an estimate of the rate at which calcium will be released to the surrounding carbonated brine. This value will be used for dimensioning the testing equipment.

ACKNOWLEDGEMENT

This work was partially supported by research grant BIA2016-76543-R from MEC (Madrid), which includes European FEDER funds, and 2017SGR-1153 from Generalitat de Catalunya (Barcelona). The first author also acknowledges her FPI scholarship (BES-2017-083000) from MEC (Madrid).

REFERENCES

[1] IPCC. Special Report on Carbon Dioxide Capture and Storage. Prepared by Working Group III of the Intergovernmental Panel on Climate Change. Cambridge University Press, Cambridge, United Kingdom and New York, NY, USA (2005).

[2] Gasda, S. E., Bachu, S. and Celia, M. A. The potential for CO_2 leakage from storage sites in geological media: analysis of well distribution in mature sedimentary basins. *Environmental Geology* (2004) **46**:6–7.

[3] Kutchko, B. G., Strazisar, B. R., Dzombak, D. A., Lowry, G. V. and Thaulow, N. Degradation of well cement by CO_2 under geologic sequestration conditions. *Environmental Science and Technology* (2007) **41**:4787–4792.

[4] Carey, J. W., Wigand, M. Chipera, S. J., WoldeGabriel, G. Pawar, R., Lichtner, P. C., Wehner, S. C., Raines, M. A. and Guthrie, G. D. Analysis and performance of oil well cement with 30 years of CO_2 exposure from SACROC Unit, West Texas, USA. *International Journal of Greenhouse Gas Control* (2007) **1**:75–85.

[5] Liaudat, J., Martínez, A., López, C. M. and Carol, I. Modelling acid attack of oilwell cement exposed to carbonated brine. *International Journal of Greenhouse Gas Control* (2018) **68**:191–202.

[6] Duguid, A. and Scherer, G.W. Degradation of oilwell cement due to exposure to carbonated brine. *International Journal of Greenhouse Gas Control* (2010) **4**:546–560.

[7] Samson, E. and Lemaire, G. Modeling chemical activity effects in strong ionic solutions. *Computational Materials* (1999) **15**:285–294.

[8] Oh, B. H. and Jang, S. Y. Prediction of diffusivity of concrete based on simple analytic equations. *Cement and Concrete Research* (2004) **34**:463–480.

[9] Idiart, A. E., López, C. M. and Carol, I. Modeling of drying shrinkage of concrete specimens at the meso-level. *Material and Structures*. (2011a) **44**:415-435.

[10] Idiart, A. E., López, C. M. and Carol, I. Chemo-mechanical analysis of concrete cracking and degradation due to external sulfate attack: A meso-scale model. *Cement and Concrete Composites*. (2011b) **33**:411–423.

[11] Liaudat, J., López, C. M. and Carol, I. Coupled C-M meso-scale model for ASR expansion in concrete, in Meschke, G., Pichler, B., Rots, J.G. (Eds.). *Computational Modelling of Concrete Structures: Proceedings of the Conference on Computational Modelling of Concrete and Concrete Structures (EURO-C 2018)*, Bad Hofgastein, Austria (2018), pp. 363–370.

[12] Rodríguez, M., López, C. M. and Carol, I. Modeling of Heat and Mass Transfer Induced by High Temperature in Concrete. In: Oñate E., Owen D.R.J., Peric D., Chiumeti M. (eds). *XIII International Conference on Computational Plasticity. Fundamentals and Applications COMPLAS XIII*. CIMNE, Barcelona (2015), pp 346-353.

[13] Dubacq, B., Bickle, M. J. and Evans, K. A. An activity model for phase equilibria in the H_2O-CO_2-NaCl system. *Geochimica et Cosmochimica Acta* (2013) **110**: 229–252.

[14] Brouwers, H. J. H. The work of Powers and Brownyard revisited: Part 1. *Cement and Concrete Research* (2004) **34**:1697–1716.

[15] Brouwers, H. J. H. The work of Powers and Brownyard revisited: Part 2. *Cement and Concrete Research* (2005) **35**:1922–1936.

[16] AENOR, Cement-part 1: Composition, Specifications and Conformity Criteria for Common Cements UNE-EN 197-1 (2011), AENOR, Madrid.

[17] Gallucci, E., Zhang, X., Scrivener, K.L. Effect of temperature on the microstructure of calcium silicate hydrate (C–S–H). *Cement and Concrete Research* (2013) **53**: 185—195.